Determination of Length Scales in Algebraic Turbulence Models for Navier-Stokes Methods

H. W. Stock* and W. Haase†
Dornier GmbH, Friedrichshafen, Federal Republic of Germany

The algebraic turbulence models that are used in today's Navier-Stokes methods have their origin in boundary-layer research. The length scales in those models are the viscous-layer thickness or other suitable boundary-layer integral quantities, which are not known a priori in Navier-Stokes calculations. Baldwin-Lomax first circumvented that problem by finding an alternative expression patterned after the Cebeci-Smith model. In the first part of the present paper, the differences between the Cebeci-Smith and the Baldwin-Lomax turbulence model are discussed on a boundary-layer basis. A novel method to evaluate the turbulent length scale in Navier-Stokes computations is described in the second part, which first allows a direct use of the Cebeci-Smith model (or any other turbulence model based on boundary-layer integral values) and, second, presents the opportunity for a mesh adaption procedure. This procedure guarantees a fixed number of mesh points inside the viscous layer and, hence, a controlled resolution of this area. Navier-Stokes results for both turbulence models in adapted and nonadapted meshes are compared to measurements on the RAE 2822 airfoil.

Nomenclature

c	= chord length
c_f	= skin friction coefficient
c_p	= pressure coefficient
D	= local diameter of diffuser
F	= function defined in Eq. (10)
$H = \delta^x/\theta$	= shape parameter
$H_i = \delta_i^x/\theta_i$	= incompressible shape parameter
k	= von Kármán constant
l	= mixing length
Re	= Reynolds number based on chord length
U,V	= mean velocity components in wall tangential and normal direction
u_τ	= friction velocity
x	= Cartesian coordinate
y	= wall normal coordinate
y^+	= law of the wall coordinate
y^x	= wall distance for which $\varepsilon_i = \varepsilon_o$
α	= diffuser half-opening angle
δ	= boundary-layer thickness
δ^x	= displacement thickness
δ_i^x	= incompressible displacement thickness
ε	= eddy viscosity
θ	= momentum loss thickness
θ_i	= incompressible momentum lost thickness
μ	= dynamic viscosity
Π	= Coles pressure gradient parameter
ρ	= density
σ	= wall friction parameter
τ	= shear stress
ω	= vorticity

Subscripts

l	= laminar
t	= turbulent
i	= diffuser inlet condition
i	= inner layer
o	= outer layer
w	= wall
e	= outer edge of the boundary layer
∞	= unperturbed flow

Superscripts

$\sim$	= separated flow
$-$	= wake flow

Introduction

THE main objective in developing turbulence models is to specify closure conditions in which the unknown Reynolds stresses of turbulence are related to known mean flow properties. The relation is established either analytically (zero equation model) or through differential equations for the transport quantities of turbulence (one- or two-equation models).

The turbulence models being in common use are not well advanced,[1] since they are essentially developed for attached boundary layers and simple shear flows.

For boundary-layer computations, the algebraic eddy viscosity model of Cebeci-Smith[2] (CSM) has found a broad application. For the computation of noncomplex flows solving the Navier-Stokes equations, it would be advantageous to use the CSM. Unfortunately, this model cannot be applied directly, since the edge of the viscous layer is not known a priori. The latter quantity, however, is needed for the formulation of the eddy viscosity in the outer layer in the CSM.

The Baldwin-Lomax[3] algebraic turbulence model (BLM), developed in 1978 and patterned after that of Cebeci-Smith,[2] is suitable for Navier-Stokes methods circumventing the difficulty of determining the outer edge of the viscous layer by the formulation of an alternative expression. Since then, the BLM has been widely used in its original form or a slightly modified form to take history effects into account.[4] In the past, boundary-layer-type results like δ^x, θ, and H were given fairly often in the literature applying either the CSM or BLM in Navier-Stokes methods without any explanation of how the viscous-layer thickness was determined.

Presented as Paper 87-1302 at the AIAA 19th Fluid Dynamics, Plasma Dynamics, and Lasers Conference, Honolulu, HI, June 8–10, 1987. Received July 9, 1987; revision received December 2, 1987.

*Head of Boundary Layer Aerodynamics.
†Senior Research Scientist.

The subject of the present paper is first to discuss the differences of the CSM and BLM on a boundary-layer basis. Second, a procedure is proposed to evaluate the turbulent length scales, allowing the direct application of the CSM in Navier-Stokes methods and, consequently, a nonarbitrary calculation of the viscous-layer thickness. Furthermore, a mesh adaption procedure is described that makes use of the computed turbulent length scales to assure a fixed number of mesh points inside the viscous wall layer.

Short Description of the Cebeci-Smith and Baldwin-Lomax Turbulence Models

The apparent turbulent viscosity μ_t is given by the sum of the molecular viscosity μ_l and the eddy viscosity ε times the density ρ:

$$\mu_t = \mu_l + \rho\varepsilon \tag{1}$$

where

$$\varepsilon = \begin{cases} \varepsilon_i \text{ for } y \le y^x \\ \varepsilon_o \text{ for } y > y^x \end{cases} \tag{2}$$

and y^x is the smallest value of y at which values from the inner and the outer formulas are equal.

The Prandtl-van Driest formulation is used in the CSM for the inner region:

$$\varepsilon_i = l^2\left|\frac{\partial U}{\partial y}\right| \tag{3}$$

with

$$l = ky[1 - e^{-y^+/A^+}] \tag{4}$$

$$y^+ = \frac{\sqrt{\rho_w|\tau_w|}\,y}{\mu_w} \tag{5}$$

where $k = 0.4$ and $A^+ = 26$.

Clauser's formulation together with Klebanoff's intermittency function F_{Kleb} is applied for the outer region in the CSM:

$$\varepsilon_o = \alpha U_e \delta_i^x F_{\text{Kleb}} \tag{6}$$

Although it varies slightly in the low-momentum Reynolds number range, the parameter α is generally admitted as a constant, $\alpha = 0.0168$, and

$$F_{\text{Kleb}} = \frac{1}{[1 + 5.5(y/\delta)^6]} \tag{7}$$

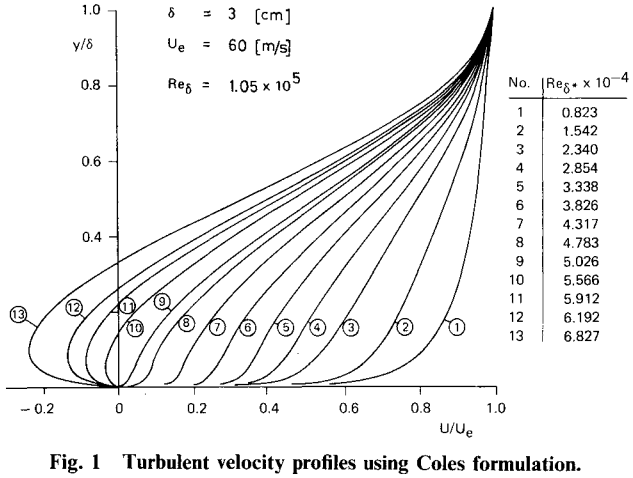

Fig. 1 Turbulent velocity profiles using Coles formulation.

For the inner region Baldwin and Lomax[3] use a formulation identical to that used by Cebeci-Smith.[2] In the outer region, however, as the length scale δ^x is not known in Navier-Stokes computations, an alternative expression is proposed:

$$\varepsilon_o = \alpha C_1 F_{\text{Kleb}}\, y_{\max} F_{\max} \tag{8}$$

or

$$\varepsilon_o = \alpha C_1 F_{\text{Kleb}}\, C_2 U_{\text{Diff}}^2 \frac{y_{\max}}{F_{\max}} \tag{9}$$

with $C_1 = 1.6$ and $C_2 = 0.25$.

The smallest value of Eqs. (8) and (9) has to be taken. The quantities $F_{\max}$ and $y_{\max}$ are determined from the function

$$F = y\left|\frac{\partial U}{\partial y}\right|[1 - e^{-y^+/A^+}] \tag{10}$$

The quantity $F_{\max}$ is the maximum value of F that occurs in a velocity profile, and $y_{\max}$ defines the y-location of $F_{\max}$.

U_{Diff} is the difference between maximum and minimum velocity in the profile

$$U_{\text{Diff}} = U_{\max} - U_{\min} \tag{11}$$

where $U_{\min}$ is taken to be zero except in wakes.

In the case of Navier-Stokes calculations, the absolute value of the velocity gradient $|\partial U/\partial y|$ in Eqs. (3) and (10) can be replaced by the absolute value of the vorticity $|\omega|$:

$$|\omega| = \left|\frac{\partial U}{\partial y} - \frac{\partial V}{\partial x}\right| \tag{12}$$

and, furthermore, the intermittency factor F_{Kleb} is given by[3]

$$F_{\text{Kleb}} = \frac{1}{[1 + 5.5(C_3 y/y_{\max})^6]} \tag{13}$$

with $C_3 = 0.3$

Comparison of Turbulence Models on a Boundary-Layer Basis

Turbulent Mean Velocity Profiles

Compared to boundary-layer experiments it is well known that the two-parameter formulation of Coles[5] is well posed to describe turbulent mean velocity profiles. The expression of Coles has been extended to also represent mildly separated flows.[6-8] Using Hinze's[9] expression for the universal wake function, the Coles velocity profiles in defect form for attached and slightly detached flows are given by

$$\frac{U_e - U}{U_e} = \frac{\sigma}{k}\left[\Pi\frac{|\sigma|}{\sigma}\left\{1 + \cos\left(\pi\frac{y}{\delta}\right)\right\} - \ln\frac{y}{\delta}\right] \tag{14}$$

where σ is defined as

$$\sigma = \frac{|c_f|}{c_f}\sqrt{\frac{|c_f|}{2}} = \frac{|\tau_w|}{\tau_w}\sqrt{\frac{|\tau_w|}{\rho_e U_e^2}} \tag{15}$$

Figure 1 gives examples of turbulent mean velocity profiles, Eq. (14), for accelerated, zero-pressure gradient and decelerated flows including separated layers. The values of the Reynolds number $Re_{\delta x}$ based on the displacement thickness δ^x for the different profiles, the velocity U_e and the boundary-layer thickness δ are additionally given. Based on these representative velocity profiles characterized by the corresponding value $Re_{\delta x}$, the differences in the CSM and BLM are shown in Fig. 2. For separated flows, a modification[10,11] is applied to the CSM to avoid an unbounded increase in ε_o; δ_i^x in Eq. (6) is

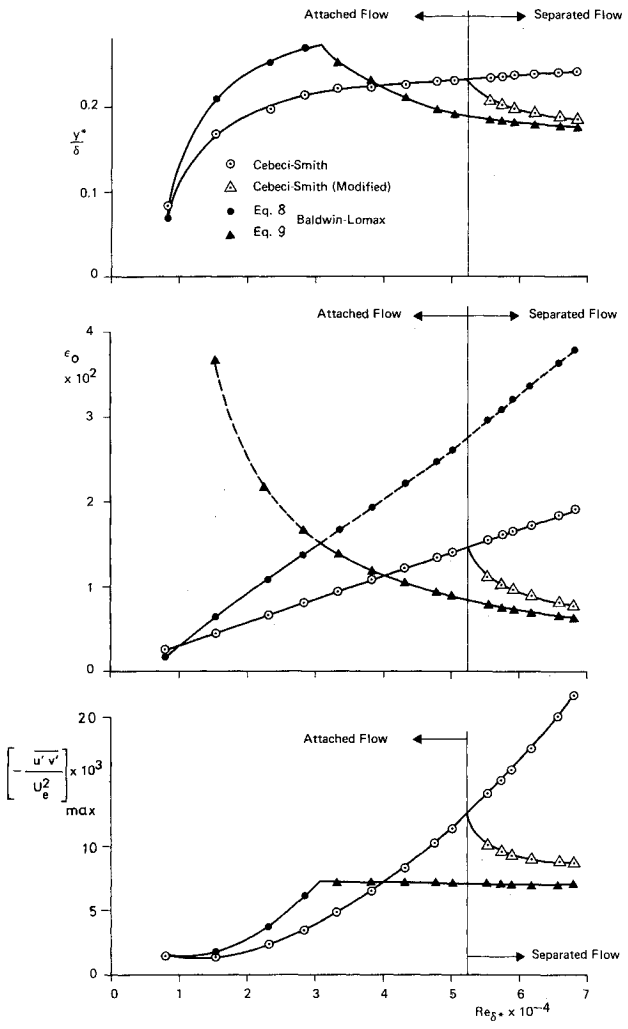

Fig. 2 Inner-layer thickness, outer-eddy viscosity, and maximum Reynolds stress as a function of the Reynolds number based on the displacement thickness.

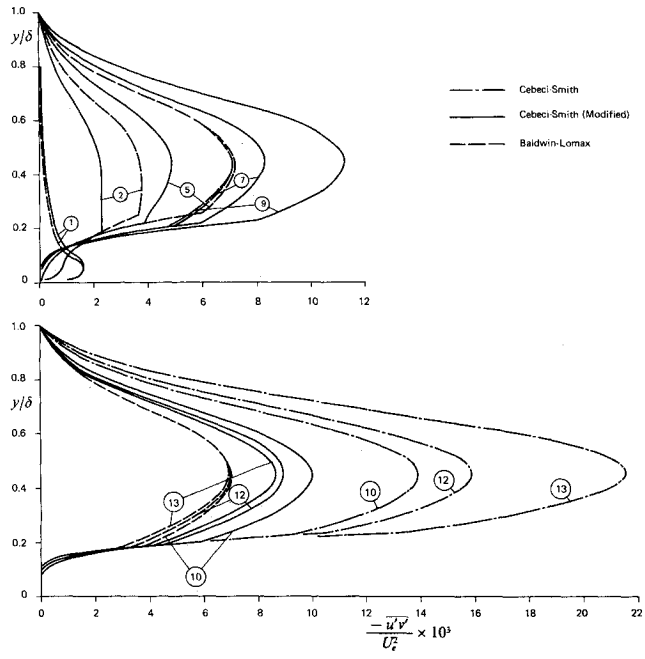

Fig. 3 Reynolds stress distribution in the boundary layer.

replaced by δ_i^x where

$$\delta_i^x = \int_{y_{U=0}}^{\delta} \left(1 - \frac{U}{U_e}\right) \mathrm{d}y \tag{16}$$

and $y_{U=0}$ is the nonzero wall distance inside the boundary layer where the velocity U is zero.

Figure 2 presents the relative wall distance y^x/δ for which ε_i equals ε_o, the eddy viscosity of the outer layer ε_o and the maximum value of the Reynolds stress component $-\overline{u'v'}$ calculated by

$$-u'v' = \varepsilon_o \left|\frac{\partial U}{\partial y}\right| \tag{17}$$

and nondimensionalized by U_e^2.

The original CSM delivers for all quantities of Fig. 2 an unbounded growth in the separated flow region. However, applying the modification, Eq. (16), the maximum values appear right at separation. The results for ε_o using the BLM with Eqs. (8) and (9) are given for demonstration purposes over the whole $Re_{\delta x}$ range. The smaller of the values ε_o should be applied; thus, the values along the dotted lines are excluded. Equation (8) of the BLM shows the same trend as the CSM. For accelerated flows, they agree well, but for zero pressure gradient or decelerated flows, all quantities are remarkably overpredicted. On the other hand, Eq. (9) of the BLM shows a similar trend on y^x/δ and ε_o compared to the modified CSM for separated flows, except that the maxima occur in regions of well attached flows, whereas the CSM delivers the maxima right at separation. Here, the value of ε_o in the BLM is approximately half of its maximum value.

The most striking fact is, however, that the maximum of the Reynolds stress $-\overline{u'v'}/U_e^2$ in the boundary layer predicted by the BLM remains for $Re_{\delta x} > 3 \times 10^4$ constant. This means that the maximum Reynolds stress is identical for all velocity profiles (nos. 5–13) in Fig. 1. Furthermore, the Reynolds stress distribution inside the boundary layer, Fig. 3, is almost identical, too, for all velocity profiles (nos. 5–13). This situation is very unlikely to be the case from known experiments. On the other hand, the Reynolds stress distribution is well overpredicted by the BLM for the velocity profiles (nos. 2–5).

The values of ε_o in Fig. 2 were computed for an intermittency factor $F_{\mathrm{Kleb}} = 1$. Figure 4 presents the F_{Kleb} distribution inside the boundary layer for both investigated models. As can be seen, the BLM does not produce intermittency at all.

In supplement, another problem occurs using the BLM in Navier-Stokes calculations. The expression for the outer layer eddy viscosity for strongly decelerated and separated flows, Eq. (9), requires the determination of $U_{\max}$ in Eq. (11). However, the evaluation of $U_{\max}$ poses some problems, because it may be located well outside the viscous layer, especially in situations where vorticity is produced in the inviscid flow region by curved or straight shocks of varying strength. In these cases, the velocity is continuously growing outside the viscous layer leading to an overprediction in $U_{\max}$ and, consequently, in ε_o. As a consequence, Eq. (8) is used for calculating ε_o, although the wall near profile behaves such that Eq. (9) should be applied.

Comparison of a Diffuser Flow Experiment with Computations Using the CSM and BLM

Both turbulence models were included in a diffuser flow calculation method,[12] which computes the boundary layer and core flow development simultaneously in one single sweep. The method uses, besides the momentum integral equation, the moment of momentum integral equation. The dissipation integral is numerically evaluated using the CSM or BLM. The computed results are compared to the Stanford Conference[13] test

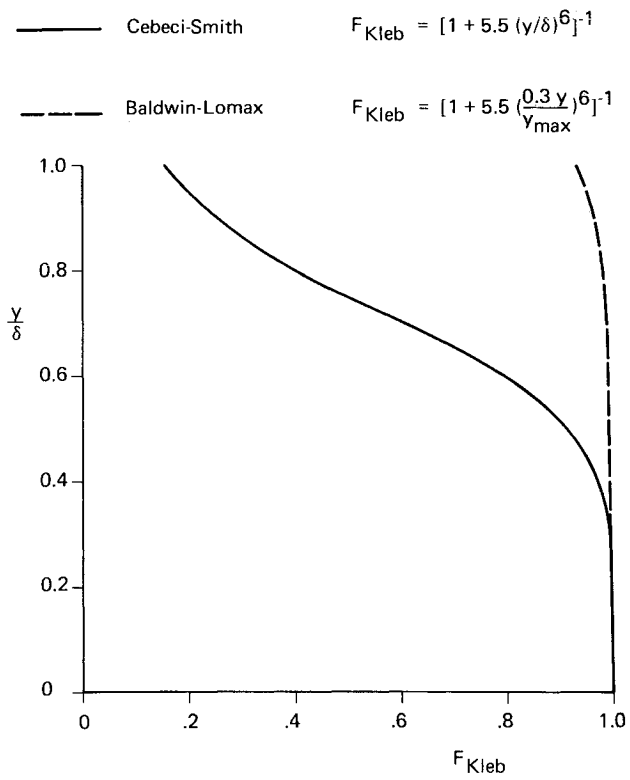

Fig. 4 Intermittency function for the Cebeci-Smith and the Baldwin-Lomax turbulence model.

case of Pozzorini[14] in Figs. 5–7. This experiment was chosen as the flow decelerates continuously nearly up to separation and is well suited with respect to the preceding discussions in showing the differences between the CSM and BLM.

Only small differences can be seen in the pressure distribution, Fig. 5, contrary to the boundary-layer properties, c_f, H, δ^x, and θ showing a distinct discrepancy. The agreement between experiments and computations is very satisfactory using the CSM. The arrows in Figs. 5 and 6 indicate the location where the BLM switches over from Eq. (8) to Eq. (9). As already discussed, Eq. (8) overpredicts ε_o with respect to the CSM; consequently, the shear stress is overpredicted, and the decay of c_f is underpredicted. Up to the arrow location, the difference between the CSM and BLM is growing. Downstream, the arrow location, Eq. (9), is valid, which first overpredicts, and approaching separation underpredicts the shear stress (see Fig. 2). At the diffuser exit, the shape parameter H (using the BLM) achieves values of about 2.5, Fig. 6, indicating that the flow approaches separation. Consequently, ε_o is underpredicted in that area, resulting in a diminishing discrepancy in skin friction between the CSM and BLM. The BLM well underestimates the shape parameter H and the displacement thickness δ^x. The momentum loss thickness θ is overpredicted by an extent, which is fairly unsatisfactory for any boundary-layer method.

Figure 7 shows a good agreement between measured and calculated velocity profiles using the CSM. The flow deceleration close to the wall is not depicted by the BLM, and the shear layer thickness is too large.

Determination of the Turbulent Length Scale for Navier-Stokes Computations

Based on the preceeding discussions, it is seen that the alternative formulation of the outer eddy viscosity ε_o in the BLM—although patterned after Cebeci-Smith[3]—does not lead to a comparable representation of ε_o in the CSM. The problem to be solved now is to find another way to compute the turbulent length scale of the viscous layer based on properties of the mean velocity profile calculated by a Navier-Stokes method.

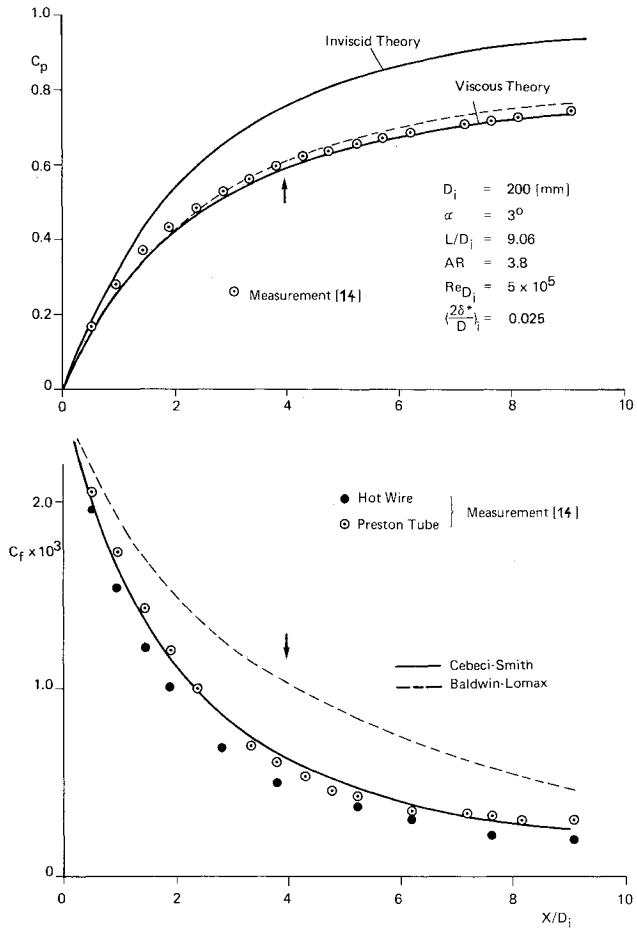

Fig. 5 Comparison of pressure and skin friction distribution with measurements for the Pozzorini diffuser test case.[14]

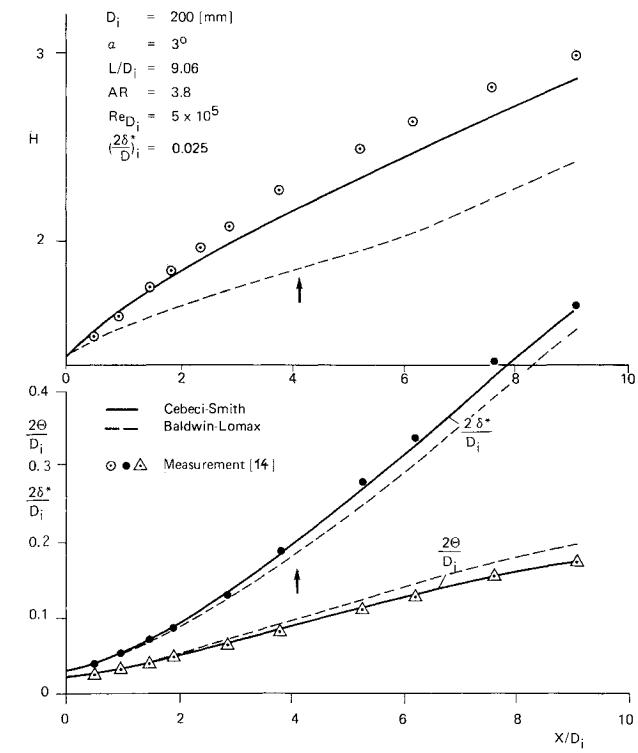

Fig. 6 Comparison of shape parameter, momentum loss, and displacement thickness with measurements for the Pozzorini diffuser test case.[14]

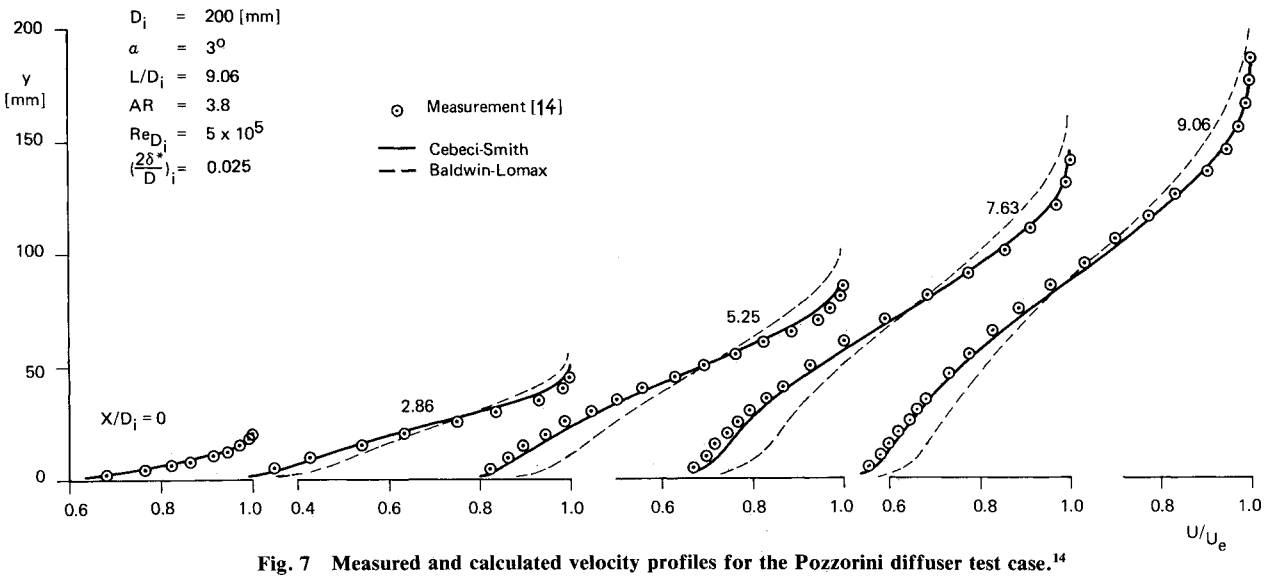

Fig. 7 Measured and calculated velocity profiles for the Pozzorini diffuser test case.[14]

Attached and Slightly Separated Wall Layers

Based on the assumption that the Coles velocity profiles[5] describe accurately enough turbulent mean flows of attached and slightly detached shear layers, it is possible to deduce a procedure enabling a direct use of the CSM in Navier-Stokes computations.

The most suitable profile property to be used is the product of the wall distance y and the velocity gradient $|\partial U/\partial y|$. From the Coles formulation, Eq. (14), which consists of a summation of the law of the wall and the law of the wake, one gets

$$y\left|\frac{\partial U}{\partial y}\right| = \frac{U_e}{k}\left[\pi|\sigma|\Pi\frac{y}{\delta}\sin\left(\pi\frac{y}{\delta}\right)+\sigma\right] \tag{18}$$

The maximum of the property $y|\partial U/\partial y|$ is given where the expression

$$Q = \frac{y}{\delta}\sin\left(\pi\frac{y}{\delta}\right) \tag{19}$$

reaches its maximum; $Q_{\max}$ is located at $y = y_{\max}$, whereby

$$\frac{y_{\max}}{\delta} = 0.646 \tag{20}$$

As seen from Eq. (18), the law of the wall delivers

$$y\left|\frac{\partial U}{\partial y}\right| = \frac{\sigma U_e}{k} = \text{const} \tag{21}$$

such that only the law of the wake contributes to the fact that the term $y|\partial U/\partial y|$ shows a maximum. The excellent situation now is that $(y|\partial U/\partial y|)_{\max}$ occurs at a constant relative wall distance inside the viscous layer, Eq. (20), for all possible flow situations—accelerated or decelerated flows and attached or detached layers.

Using that feature when analyzing the Navier-Stokes mean flow data, it is now possible to compute the desired length scale for the outer layer. Evaluating the wall distance $y_{\max}$ for which $y|\partial U/\partial y|$ or F in Eq. (10) has its maximum, delivers from Eq. (20)

$$\delta = 1.548 y_{\max} \tag{22}$$

The terms in the CSM expression for the outer layer eddy viscosity ε_o, Eq. (6), can now be calculated in the following way:

1) The velocity U_e is the velocity U at the wall distance δ.

2) Equation (7) is applied instead of Eq. (13) to calculate the intermittency factor.

3) The displacement thickness δ^x for attached flows or $\tilde{\delta}^x$, Eq. (16), for detached flows, can be evaluated either by numerically integrating the velocity profiles from $y = 0$ or $y = y_{U=0}$, respectively, to δ, or by analytically integrating the Coles velocity profiles

$$\delta_i^x = \delta\frac{\sigma}{k}[\Pi + 1] \tag{23}$$

or

$$\tilde{\delta}_i^x = \delta\frac{\sigma}{k}\left[\Pi\frac{|\sigma|}{\sigma}\left\{1 - \frac{y_{U=0}}{\delta} - \frac{1}{\pi}\sin\left(\pi\frac{y_{U=0}}{\delta}\right)\right\} - \left(\frac{y_{U=0}}{\delta} - 1\right) + \frac{y_{U=0}}{\delta}\ell n\frac{y_{U=0}}{\delta}\right] \tag{24}$$

4) The shear stress parameter σ is given by Eq. (15) where ρ_e is the density at δ, and the pressure gradient parameter Π can be deduced from Eq. (18):

$$\Pi = 0.55\left[\left(y\left|\frac{\partial U}{\partial y}\right|\right)_{\max}\frac{k}{\sigma U_e} - \frac{|\sigma|}{\sigma}\right] \tag{25}$$

Using the analytical formulation for the displacement thickness, Eq. (23), the expression for the CSM outer layer eddy viscosity can be written

$$\varepsilon_{o\text{CSM}} = \alpha U_e\frac{\delta\sigma}{k}(\Pi + 1)F_{\text{Kleb}} \tag{26}$$

The first expression Eq. (8), for ε_o in the BLM gives with Eqs. (18) and (22)

$$\varepsilon_{o\text{BLM1}} = 1.03\alpha U_e\frac{\delta\sigma}{k}(1.82\Pi + 1)F_{\text{Kleb}} \tag{27}$$

such that

$$\frac{\varepsilon_{o\text{BLM1}}}{\varepsilon_{o\text{CSM}}} \cong \frac{1.82\Pi + 1}{\Pi + 1} \tag{28}$$

For accelerated flows, the parameter Π is round about zero, which means that for this situation the BLM1 and CSM expression are identical (see also Fig. 2). For highly decelerated

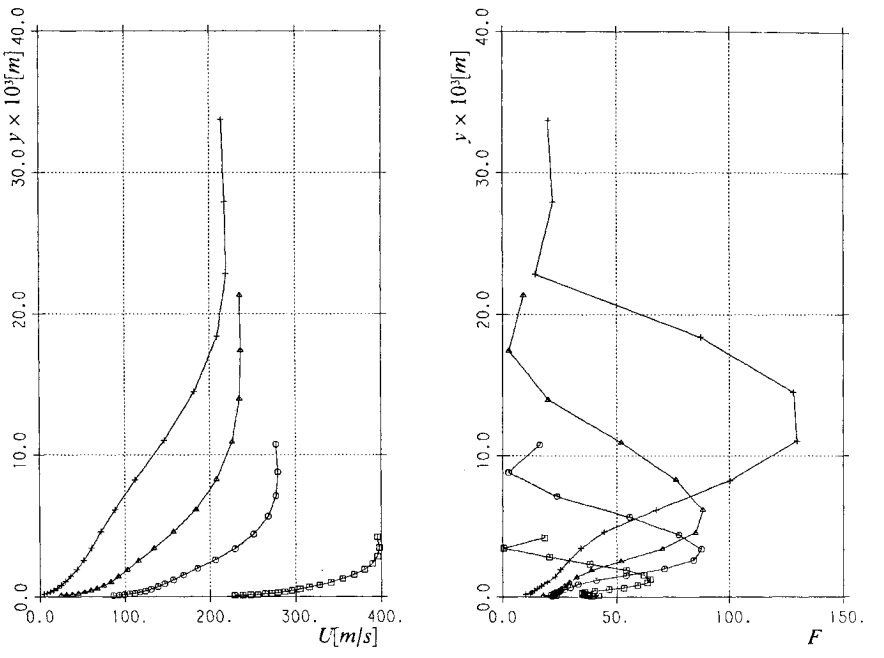

Fig. 8 Typical velocity profiles on an airfoil and the corresponding F distribution.

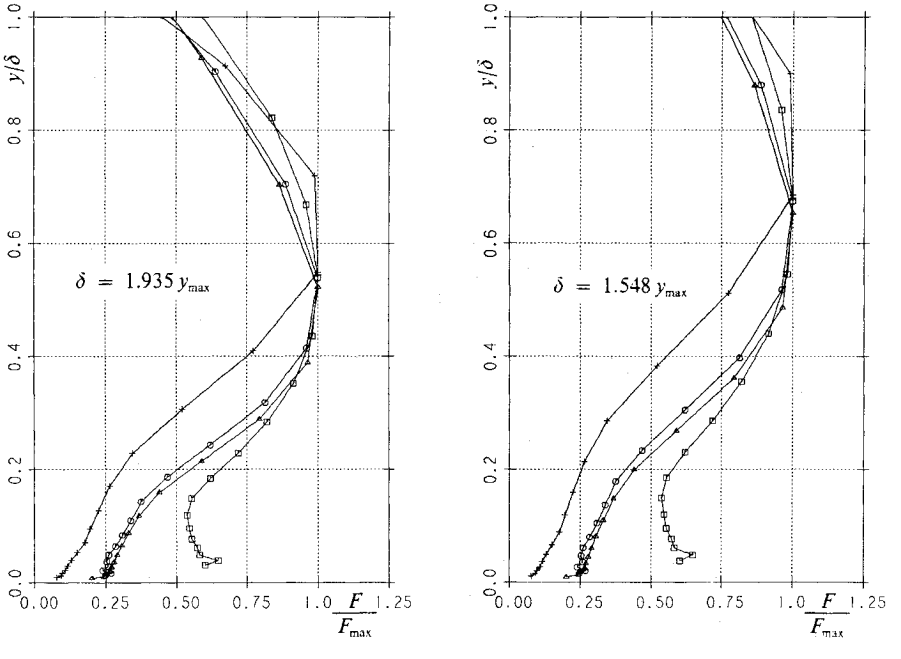

Fig. 9 Normalized F distribution using the different interpretations of the viscous-layer thickness.

flows ($\Pi \gg 1$), the BLM1 expression overpredicts ε_o by a factor of 1.82 (see also Fig. 2).

The second expression, Eq. (9), for ε_o in the BLM, which should be applied in regions where $\Pi > 1$ delivers

$$\frac{\varepsilon_{o\text{BLM2}}}{\varepsilon_{o\text{CSM}}} = \frac{0.0227}{\Pi^2\sigma^2} \tag{29}$$

Right at separation where $\sigma \to 0$ and $\Pi \to \infty$, the product $\sigma\Pi$ gives a value of $k/2 = 0.205$; hence, for this situation the BLM2 expression underpredicts ε_o by a factor of 0.554. Again, the same behavior was described in Fig. 2.

Wake Flows

In order to treat wake flows in a simple manner, a far-wake expression for the eddy viscosity may be used that equals the outer eddy viscosity ε_o, Eq. (6), for wall layers. Assuming that the law of the wake of Coles may represent wake mean velocity profiles, one can write

$$\frac{U_e - U}{U_e} = \bar{\Pi}\left[1 + \cos\left(\pi\frac{y}{\delta}\right)\right] \tag{30}$$

with

$$\bar{\Pi} = (1/2)[1 - (U_D/U_e)] \tag{31}$$

where U_D is the velocity at the wake centerline.

A similar expression as Eq. (18) gives

$$y\left|\frac{\partial U}{\partial y}\right| = \bar{\Pi}\frac{y}{\delta}\sin\left(\pi\frac{y}{\delta}\right) \tag{32}$$

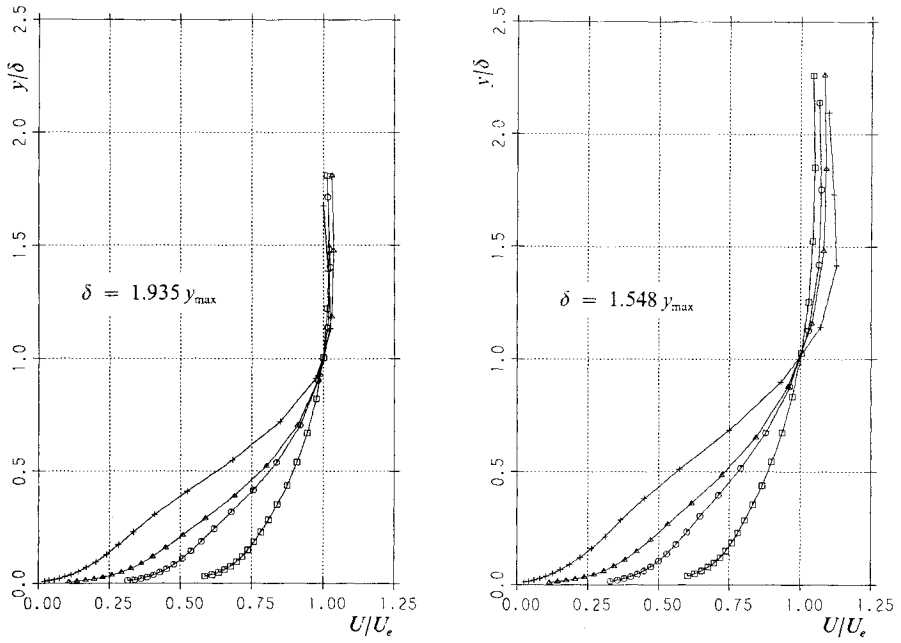

Fig. 10 Normalized velocity distribution using the different interpretations of the viscous-layer thickness.

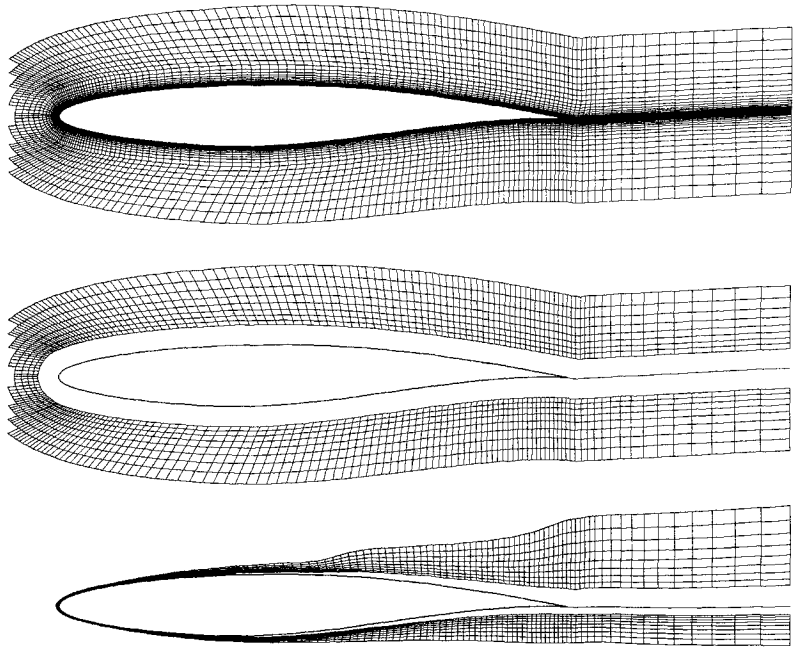

Fig. 11 Initial and adapted mesh for the RAE 2822 airfoil, case 9.[18]

such that the thickness of the wake upper and lower layer $\bar{\delta}_1$, and $\bar{\delta}_2$, respectively, are determined by the same expression as for wall layers, Eqs. (20) and (22).

The corresponding term δ_i^x in Eq. (6)—for wakes $\bar{\delta}_i^x$—can be evaluated by numerical integration or analytically from

$$\bar{\delta}_i^x = \delta \bar{\Pi} \tag{33}$$

Final Expression for the Turbulent Length Scale

Applying the CSM together with the turbulent length scale expression, Eq. (22), and a numerical integration of the velocity profile for δ_i^x has shown in all trial Navier-Stokes calculations a systematic underprediction of the viscous-layer thickness. By analyzing numerous computed velocity profiles, it was seen that by increasing the constant parameter in Eq. (22) by 25%

$$\delta = 1.936 y_{max} \tag{34}$$

the viscous-layer thickness was predicted well.

The results in Figs. 8–10 support the updating of the turbulent length scale, Eq. (34). Figure 8 presents several velocity profiles on the upper surface of an airfoil at angle of attack in transonic flow (Navier-Stokes results). The right-hand side in Fig. 8 shows the corresponding F distribution, Eq. (10). The ratio F/F_{max} vs the relative wall distance y/δ is presented in Fig. 9, whereby the right part of the figure shows δ being evaluated from the original expression, Eq. (22), and the left diagram gives the distribution based on the corrected equation, Eq. (34). The numerical value of F_{max} and the wall distance y_{max} at which it occurs was found by a spline-fit procedure. The corre-

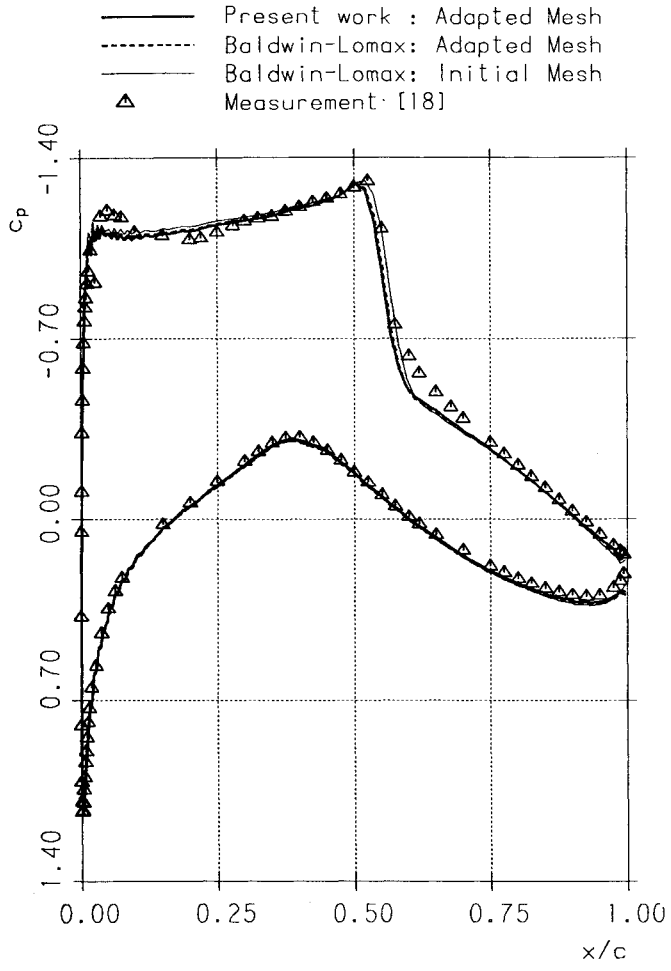

Fig. 12 Measured and calculated pressure distribution for the RAE 2822 airfoil, case 9, for $M = 0.73$ and $\alpha = 2.79$ deg.[18]

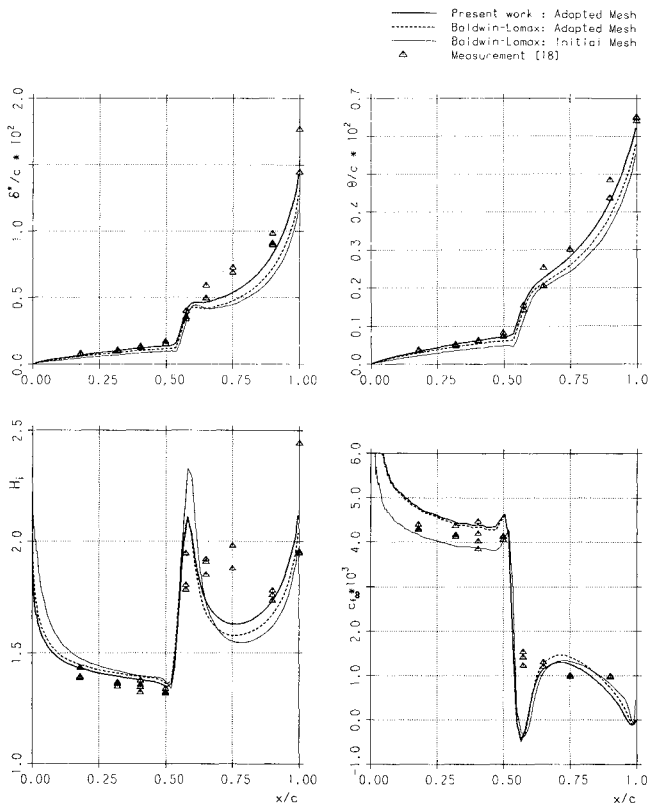

Fig. 13 Calculated boundary-layer properties compared to measurements for the RAE 2822 airfoil, case 9, for $M = 0.73$, and $\alpha = 2.79$ deg.[18]

sponding velocity profiles U/U_e vs y/δ are depicted in Fig. 10. Here again, δ is deduced from the original expression (right part of Fig. 10) and from the corrected formula (left part of Fig. 10). As it may be seen easily, the correction, Eq. (34), gives a clearly superior representation of the viscous-layer thickness. Furthermore, the aforementioned statement concerning the relative location of F_{max} inside of the viscous layer being independent of the velocity profile shape, seems to be proved by the results of Fig. 10.

Results Obtained by Solving the Time-Averaged Navier-Stokes Equations

Navier-Stokes Method

In the present investigation, the numerical method to solve the Navier-Stokes equations for compressible flows in full conservation form is a finite-volume method according to Ref. 15. Rewriting the governing equations in integral form and dividing the computational domain into quadrilateral cells, one obtains a system of ordinary differential equations by applying the integral equations to each cell separately.[15] The set of ordinary differential equations in time is solved by means of an explicit three-stage Runge-Kutta-type time-stepping method. To control an odd-even decoupling, a blended second- and fourth-order filter is introduced. Because only the steady state is of interest, the difference equations are solved by a local time-stepping approach based on the maximum allowable time step for each cell (CFL number = 1.8). Introducing the residual-averaging approach,[16] i.e., collecting the information from residuals implicitly, gives rise to a higher CFL number that has been chosen to be 3.5 in all calculations. The viscous terms are treated using central differences throughout the domain and one-sided formulas at the surface.

The steady state is defined to be reached if all force coefficients do not vary by more than 0.05%, and for transonic flow problems the total number of supersonic points remains constant within a monitoring sequence of 30 iterations. Typically, an error norm reduction ($L2$-norm of $\partial\rho/\partial t$) of approximately four decades is then obtained.

Performing an Adapted Mesh Based on Viscous-Flow Data

The advantage of the new turbulent length scale computation is twofold. First, the CSM can be applied directly and, second, an adapted mesh can be established during the course of iterations based on the knowledge of the shear layer thickness δ. Hence, it is possible to ensure a constant desired mesh point number inside the viscous layer from the leading edge of the airfoil down to the wake, producing a controlled resolution in this area. Additionally, the wake centerline is equally well adapted to the numerically evaluated streamline leaving the airfoil trailing edge[19] during the iteration.

The total number of mesh points inside the viscous layer was chosen to $n = 25$ for all test cases. These points are aligned in the wall normal direction or, in the wake, nearly normal to the wake centerline. For wall layers, the height of the first volume adjacent to the wall is chosen such that the value y^+ for the considered volume center satisfies the condition

$$y_1^+ = \frac{y_1 |u_\tau|}{\nu_W} = 1 \tag{35}$$

With respect to the volume heights, a geometrical stretching is used across the viscous layer with a constant ratio q of neighboring volume heights. The mesh in the inviscid region is generated by simple stretching functions.

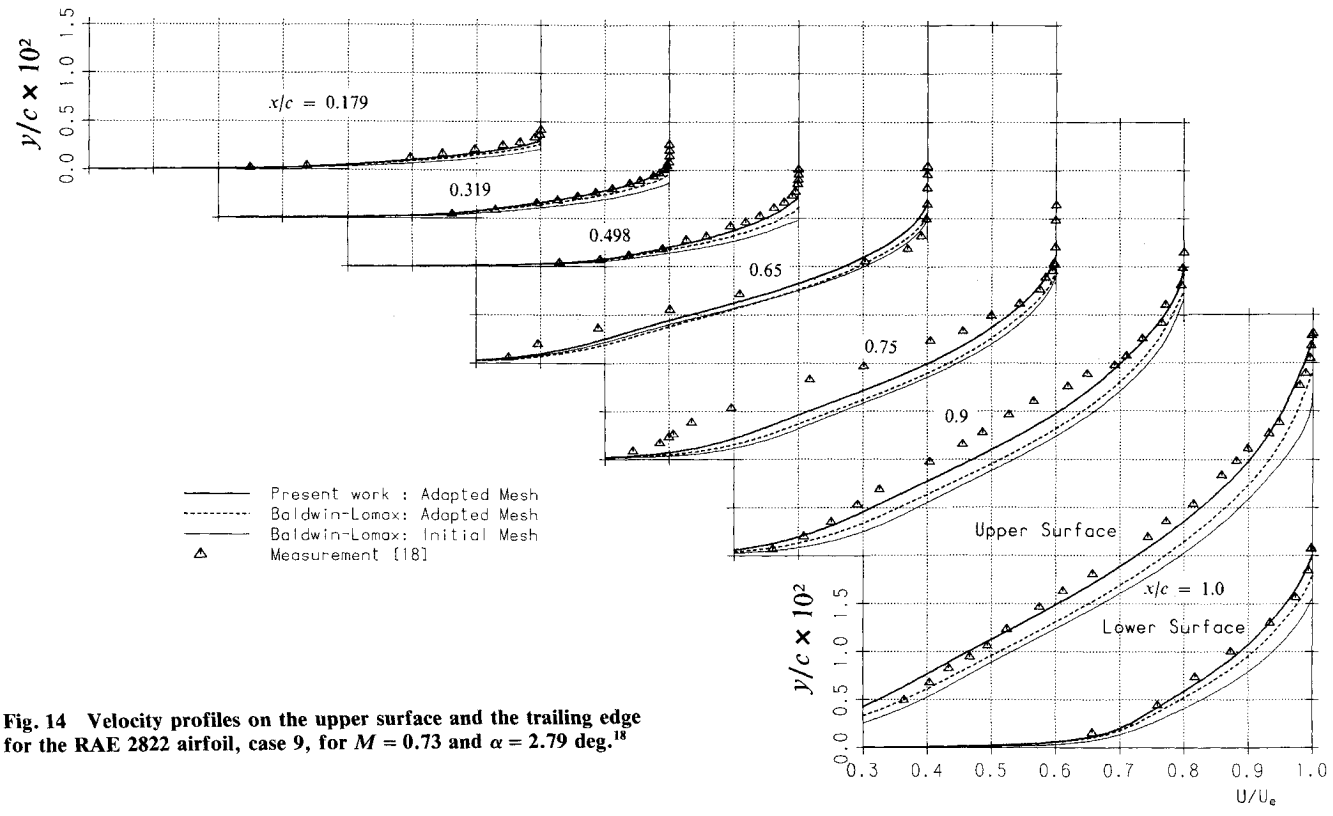

Fig. 14 Velocity profiles on the upper surface and the trailing edge for the RAE 2822 airfoil, case 9, for $M = 0.73$ and $\alpha = 2.79$ deg.[18]

In order to update the mesh during the course of iterations, the computed quantities δ and u_τ on the airfoil and in the wake are smoothed by use of a Shuman filter. The present updating of the mesh delivers a redistribution in a normal direction along the airfoil and the wake centerline. A supplementary updating in a wall tangential direction as proposed in Ref. 17 was not applied in the present calculations.

Figure 11 gives an example of the mesh updating for the RAE 2822 airfoil,[18] case 9. In the upper part of the Fig. 11, the initial mesh in the vicinity of the airfoil is presented. In the middle of Fig. 11, the first 25 volumes adjacent to the wall were omitted. The finally (three times) updated mesh is given in the lower part of Fig. 11. The empty space between airfoil/wake and the first mesh line parallel to airfoil and wake represents the calculated viscous-layer thickness and consists of the desired 25 volumes normal to the wall and wake centerline. As may be seen, the present updating already carries some of the computed flow features, i.e., the rapid growth of the viscous layer approaching the trailing edge and the nicely detectable shock wave boundary-layer interaction zone.

RAE 2822 Airfoil Results (Case 9)

The transonic flow around the RAE 2822 airfoil was calculated at a Mach number $M = 0.73$, a Reynolds number based on the chord length of $Re = 6.5 \times 10^6$, and at a corrected[18] angle of attack $\alpha = 2.79$ deg. Three different computational results will be given in Figs. 12–14.

First, the flow was computed using the CSM together with the present turbulent length scale calculation and the adapted mesh given in the lower part of Fig. 11 (298 × 70 mesh points, 204 on the airfoil). The second calculation uses the BLM in the initial mesh (mesh point number as in the adapted mesh), and the third computation has been performed again with the BLM, but in the adapted mesh. It should be kept in mind that the third calculation is only given for comparison, as the BLM works without any information about the viscous-layer thickness. All three calculations were done with a small filter value, keeping the numerical viscosity down and thus tolerating only small oscillations in the solution. In all calculations the numerically integrated value of δ_i^x and $\bar{\delta}_i^x$ were used.

Figure 12 gives the pressure distribution compared to the measurements. The calculations are almost identical except in the shock location and the plateau pressure on the suction surface. They do not represent sufficiently well the small suction peak in the nose region on the upper surface. A possible explanation may be the fact that the largest differences between the design and the actual airfoil contour are located in that region (the design contour was used for all computations). Furthermore, the compression of the flow in the shock region is overpredicted, which is certainly due to the deficiencies of the turbulence models in strong interaction regions. Figure 13 shows the boundary-layer-type results $\delta_i^x\theta$, H_i, and c_f. These results using the BLM model could only be obtained by analyzing the final converged flowfield data by the present approach to determine the viscous-layer thickness.

The best agreement with the measured data is found with the CSM model together with the present turbulent length scale calculation. Especially upstream of the shock, the BLM clearly underpredicts the displacement and momentum loss thickness. This situation is ameliorated by the use of the adapted mesh. In the shock region, due to the lack of an interaction turbulence model, the incompressible shape parameter H_i is clearly overpredicted, and the subsequent relaxation of H_i is not seen in the experiment. The corresponding underprediction of δ^x in the region downstream of the shock is responsible for the overestimation of the compression in that region (see Fig. 12).

The calculated and measured velocity profiles at different x/c stations are presented in Fig. 14. Here again, the results of the present work are visibly in better agreement with the measurement. Upstream of the shock and in the trailing-edge region the prediction also is fairly acceptable for the lower-side trailing-edge flow.

Conclusions

1) On the basis of boundary-layer results it is shown that a considerable discrepancy exists between the algebraic turbulence models of Cebeci-Smith and Baldwin-Lomax. The turbulent shear is overpredicted by the Baldwin-Lomax model for mildly decelerated flows and underpredicted for flows approaching separation.

2) The novel method to predict the turbulent length scale, i.e., the viscous-layer thickness is very easy to apply and delivers a good agreement with measurements.

3) The turbulent length scale calculation allows to apply each algebraic turbulence model based on a length scale in Navier-Stokes calculations. Furthermore, the generation of adapted meshes is possible, which guarantees a fixed number of mesh points inside the viscous layer and, hence, a controlled resolution of this area.

4) The Baldwin-Lomax turbulence model can be applied directly in Navier-Stokes calculations, but it seems to produce deviations with respect to experiments in boundary-layer as well as in Navier-Stokes computations. On the other hand, the use of the Cebeci-Smith turbulence model in Navier-Stokes methods without a prediction basis for the turbulent length scale is, strictly speaking, open to any interpretation of the user. Only the combination of the presented turbulent length scale prediction method together with the Cebeci-Smith model delivers, as shown, satisfactory results.

References

[1]Marvin, J. G., "Turbulence Modeling for Computational Aerodynamics," AIAA Paper 82-0164, Jan. 1982.

[2]Cebeci, T. and Smith, A. M. O., *Analysis of Turbulent Boundary Layers*, Academic, New York, 1974.

[3]Baldwin, B. S. and Lomax, H., "Thin Layer Approximation and Algebraic Model for Separated Turbulent Flows," AIAA Paper 78-257, Jan. 1978.

[4]Visbal, M. and Knight, D., "Evaluation of the Baldwin-Lomax Turbulence Model for Two-Dimensional Shock Wave Boundary Layer Interactions," AIAA Paper 83-1697, July 1983.

[5]Coles, D., "The Law of the Wake in Turbulent Boundary Layer," *Journal of Fluid Mechanics*, Vol. 1, Pt. 2, Feb. 1956, pp. 191–226.

[6]Kuehn, G. D. and Nielsen, J. N., "Prediction of Turbulent Separated Boundary Layers," AIAA Paper 73-663, July, 1973.

[7]Assassa, G. M. and Gay, B., "Prediction Numérique des Ecoulements Turbulents au Voisinage du Point de Décollement," *J. Entropie*, No. 81, May/June 1978, pp. 29–38.

[8]Bower, W. W., "Analytical Procedure for Calculation of Attached and Separated Subsonic Diffuser Flows," *Journal of Aircraft*, Vol. 13, Jan. 1976, pp. 49–56.

[9]Hinze, J. O., *Turbulence*, McGraw-Hill, New York, 1959.

[10]Alber, I. E., "Similar Solutions for a Family of Separated Turbulent Boundary Layers," AIAA Paper 71-203, Jan. 1971.

[11]Rubesin, M. W., Okonu, A. F., Levy, L. L., Devitt, J. B. and Seegmiller, H. L., "An Experimental and Computational Investigation of the Mean and Dynamic Flow Field about an Airfoil in Supercritical Flow with Turbulent Boundary Layer Separation," International Council of the Aeronautical Sciences, Paper 76-15, Oct. 1976.

[12]Stock, H. W., "Compressible Turbulent Flows in Long Circular Cross-Section Diffusers of Large Area Ratio," *Zeitschrift für Flugwissenschaften und Weltraumforschung*, Vol. 9, No. 3, May/June 1985, pp. 143–155.

[13]Kline, S. J., Cantwell, B. J., and Lilley, G. M., "Proceedings, 1980–81, AFOSR-HTTM-Stanford Conference on Complex Turbulent Flows," Thermosciences Div., Mechanical Engineering Dept., Stanford Univ., Stanford, CA, 1981.

[14]Pozzorini, R., "Das turbulente Strömungsfeld in einem langen Kreis-Kegel Diffusor," Abhandlung der ETH Zürich, Switzerland, Dissertation 5646, ETH Zürich, 1976.

[15]Haase, W., Wagner, B., and Jameson, A., "Development of a Navier-Stokes Method Based on a Finite Volume Technique for the Unsteady Euler Equations," *Notes on Numerical Fluid Mechanics*, Vol. 7, Vieweg Verlag, Braunschweig, Germany, 1984, pp. 99–107.

[16]Jameson, A. and Schmidt, W., "Some Recent Developments in Numerical Methods for Transonic Flows," *Computer Methods in Applied Mechanics and Engineering*, Vol. 51, 1985, pp. 467–493.

[17]Haase, W., Misegades, K., and Naar, M., "Adaptive Grids in Numerical Fluid Dynamics," *International Journal for Numerical Methods in Fluids*, Vol. 5, June 1985, pp. 515–528.

[18]Cook, P. H., McDonald, M. A., and Firmin, M. C. P., "Aerofoil RAE 2822—Pressure Distributions, and Boundary Layer and Wake Measurements," AGARD-AR-138, 1979.

[19]Haase, W., "Influence of Trailing Edge Meshes on Skin Friction in Navier-Stokes Calculations," *AIAA Journal*, Vol. 24, Sept. 1986, pp. 1557–1559.